PCCP

ROYAL SOCIETY OF CHEMISTRY

PAPER

View Article Online
View Journal | View Issue

Cite this: *Phys. Chem. Chem. Phys.*, 2021, **23**, 7777

Formation of HCN^+ in collisions of N^+ and N_2^+ with a self-assembled propanethiol surface on gold†‡

Faro Hechenberger, [a] Siegfried Kollotzek, [a] Lorenz Ballauf, [a] Felix Duensing, [a] Milan Ončák, [a] Zdenek Herman*[ab] and Paul Scheier [a]

Received 6th August 2020,
Accepted 8th September 2020

DOI: 10.1039/d0cp04164e

rsc.li/pccp

Collisions of N^+ and N_2^+ with C3 hydrocarbons, represented by a self assembled monolayer of propanethiol on a polcrystalline gold surface, were investigated by experiments over the incident energy range between 5 eV and 100 eV. For N^+, formation of HCN^+ is observed at incident energies of projectile ions as low as 20 eV. In the case of N_2^+ projectile ions, the yield of HCN^+ increased above zero only at incident energies of about 50 eV. This collision energy in the laboratory frame corresponds to an activation energy of about 3 eV to 3.5 eV. In the case of N^+ projectile ions, the yield of HCN^+ was large for most of the incident energy range, but decreased to zero at incident energies below 20 eV. This may indicate a very small energy threshold for the surface reaction between N^+ and C3 hydrocarbons of a few tenths of an eV. Such a threshold for the formation of HCN^+ may exist also for collisions of N^+ with an adsorbed mixture of hydrocarbon molecules.

Introduction

Interstellar hydrogen cyanide (HCN) was discovered in 1971 by Snyder and Buhl[1] by its radio emission. It is one of the most abundant high dipole moment molecules found in space.[2] The luminosity of HCN is a tracer of dense molecular gas, which often is associated with star-forming giant molecular cloud cores.[3] In addition, HCN has been detected in many comets[4] as well as in planetary atmospheres,[5–7] brown dwarfs[8] and the atmosphere of Titan.[9–12] Hydrogen cyanide is a key molecule for the production of molecular building blocks of life and played an essential role in Earth's early atmosphere.[13–15] Electron[16] and photoionization[17] of HCN lead predominantly to the formation of the molecular cation HCN^+ and electron attachment leads to the formation of CN^- as the only anionic product.[18,19] In the present study, we are investigating the formation of the cation HCN^+ upon impact of N^+ and N_2^+ with a well-defined self-assembled monolayer (SAM) surface.

In our previous publications[20–23] we reported on studies of collisions between projectile ions Ar^+, N^+ and N_2^+ with residual gas hydrocarbons, covering surfaces of tungsten, carbon, and beryllium. In these studies, we observed the formation of HCN^+ in heterogenous reactions between the projectile ions N^+ and N_2^+ and hydrocarbons adsorbed to the metal surfaces. These hydrocarbon molecules originate from cracked pump oil residuum, usually assumed to be formed mostly by C7 and C8 hydrocarbons. The results may have a certain relevance to heterogenous chemical reactions of ions with aerosols in the atmosphere of Titan. These aerosols are referred to as tholins and only their elemental composition (C, H, N) is known from pyrolytic analysis.[12] The residual gas hydrocarbons were assumed to be at least a first approximation to those mysterious tholins. The former experiments were carried out on the Innsbruck apparatus BESTOF, described in ref. 24. It consisted of two mass spectrometers arranged in tandem geometry and composed of the following parts: an electron impact ion source to form projectile ions, a two-sector field mass spectrometer to select a specific projectile ion, a metal or carbon target surface covered with hydrocarbons, a system to extract pulses of product ions, a linear time-of-flight analyser for the product ions and a multichannel-plate detector. The intensity of the projectile beam was fairly low and the sputtering of hydrocarbons from the surface was slow. The hydrocarbon coverage was thus quite stable and constantly renewed from the hydrocarbons present in the residual gas. However, such a hydrocarbon surface does not represent a well-defined target and an extension of these experiments requires better-defined surfaces. Such a surface can be provided by self-assembled

[a] *Institut für Ionenphysik und Angewandte Physik, Universität Innsbruck, Technikerst. 25, A-6020 Innsbruck, Austria. E-mail: paul.scheier@uibk.ac.at*
[b] *J. Heyrovský Institute of Physical Chemistry, V.V.i, Academy of Sciences of the Czech Republic, Dolejškova 3, 18223 Prague 8, Czech Republic*

† We dedicate this paper to Jan Peter Toennies on the occasion of his 90th birthday. One of us (Z. H.) cannot find words to express the depth of his admiration and gratitude to Peter, the senior friend and colleague of more than fifty years.

‡ Electronic supplementary information (ESI) available. See DOI: 10.1039/d0cp04164e

monolayer (SAM) samples prepared according to procedures published in the literature.[25,26]

Thiol SAMs on gold are frequently used for building systems and devices for nanotechnology, including nanodevices and molecular electronics,[27] micro- and nanofabrication,[28] molecular recognition,[29] biomimetic systems[30] and to stabilize and/or functionalize metal nanoparticles.[31,32] For our first study with a defined surface, a self-assembled monolayer of propanethiol on a gold surface was chosen. In this way, collisions between the projectile ions Ar^+, N^+ and N_2^+ with a C3 hydrocarbon chain could be investigated. In the meantime, however, BESTOF, the apparatus for studying reactive ion-surface collisions, was replaced by a considerably more advanced machine, designated SurfTOF (Surface Time-of-flight Mass Spectrometer).[33] The main advantages of this new apparatus are higher sensitivity, higher resolution, better vacuum conditions, and much higher intensity of the incident projectile beam then the apparatus BESTOF could provide (by several orders of magnitude).

Experimental

The new apparatus SurfTOF and its performance were in detail described elsewhere.[33] Briefly, projectile ions from an electron impact source are mass-per-charge selected using a quadrupole Pfeiffer QMA 400 filter. The projectile beam then hits the surface (in the experiments described here under an angle of 45°) with an incident energy adjustable from a few eV to several hundred eV. Ions emerging from the collisions are extracted from the surface region, focused into a beam and guided to a second mass spectrometer system for analysis. In order to maximize the yield of product ions, the distance from the surface to the analysing mass spectrometer system is kept as short as possible and the acceptance angle of the lens system as large as possible. The ions are accelerated and focused on the entrance of an orthogonal extraction reflectron time of flight mass spectrometer. The ions are detected by a set of two multichannel plates forming a chevron stack. The rigorous use of computer aided design software during the development of this instrument is responsible for the successful performance of the new device (see Fig. 1).

The SAM of propanethiol was prepared by immersing a clean gold substrate into a propanethiol solution.[34] The target surface for SurfTOF was a polycrystalline gold sheet 15 × 5 × 0.7 mm (purity of 99.97% from Ögussa GmbH) and for the STM analysis of the SAM we used a single crystal Au(111) sample (purity 99.999% from MaTecK). Although self-assembly takes place rapidly, several experimental procedures are required to produce consistent, highly ordered films.[35] A clean environment is key to preparing high-quality SAMs. The gold surface as well as all glass containers and tools were cleaned with piranha solution (70 : 30 v/v solution of 70% concentrated sulfuric acid and 30% hydrogen peroxide). For thiol compounds, the most common method is to put the gold surface in deoxygenated ethanol at a total concentration of thiol of 1 to 5 mM.[35] We stored the samples for 24 h at room temperature which resulted in perfect monolayer

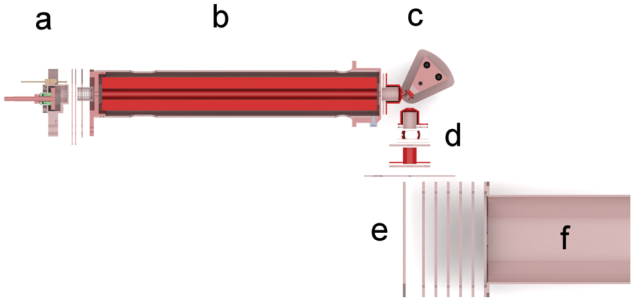

Fig. 1 Schematic of the apparatus SurfTOF with the major parts labelled; (a) electron impact ion source, (b) quadrupole mass filter, (c) heated target surface, (d) ion optics and second electron impact ion source, (e) orthogonal extraction region of a reflectron TOF-MS, (f) drift tube of the TOF-MS.

packing as indicated by the STM image of a propanethiol SAM on a single crystal Au(111) surface (see Fig. 2). After rinsing the SAM samples with ethanol and drying them in a stream of dry nitrogen gas, we transferred the samples into the ultra-high vacuum of the STM or SurfTOF. All samples were irradiated with a projectile ion current of 1.4 nA for better comparison of different projectile ions. Table 1 compares the pressures, ion fluence and dose rate per molecule of SurfTOF with the previous setup BESTOF.[20,24]

Results

Fig. 2 shows four STM images before (left) and after (right) the attachment of propanethiol SAMs to Au(111) (top) and the polycrystalline gold surface (bottom) used as the target in SurfTOF. All images cover the same area of 2 × 2 nm. Fig. 2a shows the clean atomically flat region of Au(111). A regular

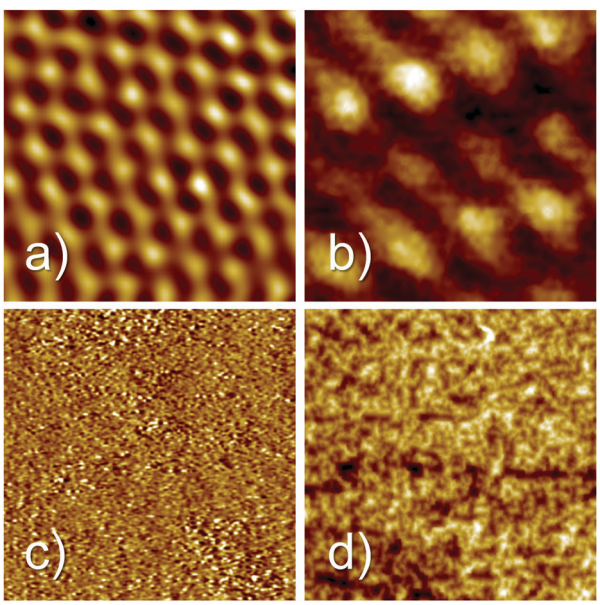

Fig. 2 2 × 2 nm^2 STM images before (left column) and after (right column) the attachment of a propanethiol SAM on Au(111) (upper images, imaging parameters: I_t = 1.06 nA, U_{bias} = 0.88 V) and the polycrystalline gold SurfTOF surface (lower line, I_t = 0.33 nA, U_{bias} = 1.35 V).

Table 1 Comparison of the experimental parameters used in the present study (SurfTOF) and the previous experimental setup (BESTOF) utilized by Harnisch *et al.*[20]

	SurfTOF	BESTOF[20]
Base pressure surface	2×10^{-6} Pa	10^{-6} Pa
Base pressure ion source	1.4×10^{-6} Pa	2×10^{-6} Pa
Pressure surface beam on	3×10^{-6} Pa (7×10^{-6} N^+)	3×10^{-6} Pa
Pressure ion source beam on	3×10^{-5} Pa (3×10^{-4} N^+)	4–9 $\times 10^{-3}$ Pa
Projectile ion fluence	10^{10} s^{-1} mm^{-2}	10^{8} s^{-1} mm^{-2}
Dose rate per molecule	2×10^{-3} s^{-1}	2×10^{-5} s^{-1}

pattern with a substantially larger unit cell can be seen for the propanethiol SAM grown on the Au(111) surface. The maximum coverage of thiolate than can be achieved on Au(111) is 1/3 ML. At this coverage and room temperature, a $\sqrt{3} \times \sqrt{3}$ $R30°$ phase is often found for alkanethiol monolayers.[36,37] However, the coverage observed in Fig. 2b is much lower. Compared with the literature,[36–38] the structure seen is likely to be a $4 \times \sqrt{3}$ phase where the sulphur heads occupy every second position in one direction ($\sqrt{3}$ times the lattice distance of Au(111)) but only every fourth position in the other direction (4 times the lattice distance of Au(111)). Fig. 2c shows an STM image of a clean polycrystalline gold surface. Due to the roughness of the sample, no atomic resolution could be achieved. The same is true also after covering the surface with a propanethiol SAM (Fig. 2d).

In order to probe the degradation of the SAM upon ion irradiation, we measured the temporal behavior of $C_2H_3^+$, S^+ and Au^+ in the secondary ion mass spectra upon 1.4 nA Ar^+ bombardment at 69 eV collision energy for almost 17 hours. The ion yield at m/z = 32 consists of two isobaric ions (see Fig. S1 in the ESI‡). For the evaluation, we only used the lighter peak that we assigned to S^+. The yields of the two products from propanethiol, *i.e.*, $C_2H_3^+$ and S^+ decrease more than an order of magnitude within the first hour. In the case of S^+ (red dashed line in Fig. 3), the data follow nicely a simple exponential

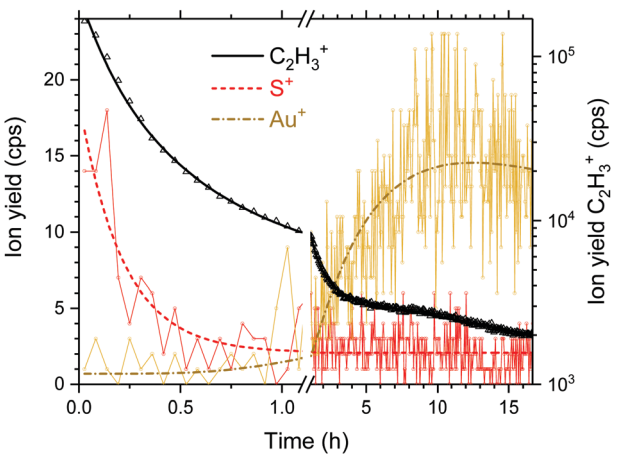

Fig. 3 Temporal evolution of the fragment ions S^+ and $C_2H_3^+$ of propanethiol and sputtered Au^+ from the Au(111) substrate upon long-term Ar^+ irradiation at 69 eV and 1.4 nA.

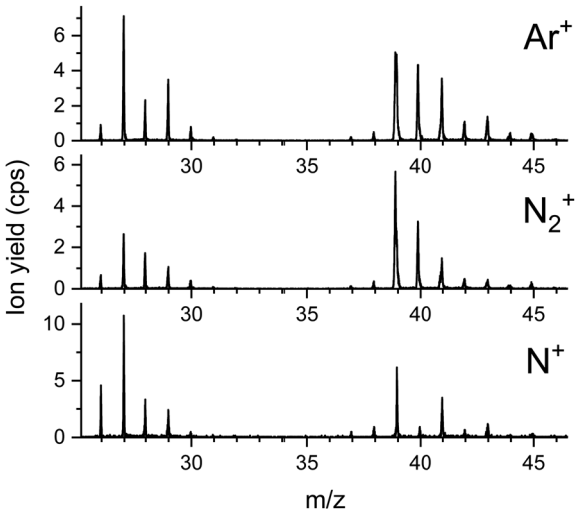

Fig. 4 Sections of product ion mass spectra obtained for three different projectile ions colliding at 100 eV onto a propanethiol SAM on Au(111).

decrease, whereas the yield of $C_2H_3^+$ (black solid line in Fig. 3) decreases even more rapidly. Please note that the left logarithmic y-axis belongs to these data. The yield of sputtered Au^+ ions rises after one hour above the noise level. We consider at this the SAM to be completely sputtered off the gold surface. All following measurements were performed at freshly prepared SAM samples with irradiation times substantially shorter than one hour which required frequent replacement of target samples.

In Fig. 4 the same section of three mass spectra of product ions from collisions of Ar^+, N^+ and N_2^+ with the propanethiol surface at a collision energy of 100 eV are shown. It is interesting to note that Ar^+ irradiation of the SAM produces more $C_2H_x^+$ than $C_3H_x^+$ fragments. According to quantum chemical calculations shown in the ESI,‡ the C–S bond is weaker compared to the C–C bonds. This is observed for the free propanethiol molecule and for the radical attached to a gold cluster. For corresponding cationic system, the relative dissociation energy of various bonds is more evenly distributed. This can explain, along with steric hinderance due to the presence of neighbouring propanethiol molecules on the surface, the increased probability of C–C bond dissociation observed in the experiment.

The spectrum from Ar^+ collisions shows predominantly hydrocarbon ions sputtered from the SAM surface. At m/z = 40 some scattered Ar^+ projectiles are measured. The spectra from N^+ and N_2^+ collisions show the same hydrocarbon ions and a considerably increased yield at m/z = 27, indicating the formation of HCN^+. The ion yield at m/z = 28 is enhanced relatively to m/z = 29 for both N^+ and N_2^+ bombardment of the propanethiol SAM. In the case of N_2^+ this is predominantly due to scattered projectile ions. In the case of N^+, this is singly charged molecular nitrogen which originates from a small amount of N_2^{2+} projectiles that are partially neutralized upon surface collisions. In addition, N^+ collisions with the SAM lead to substantial formation of CN^+ at m/z = 26. All three projectile ions produce the same relative amounts of $C_3H_x^+$ ions (x = 3 to 6). For Ar^+, the scattered projectile ions and sputtered K^+ ions are clearly present and for

N_2^+ the peak positions of lighter isobaric ions indicate the formation of $C_2H_xN^+$ (x = 1 to 3). Due to the importance and high intensity of HCN^+, we concentrate now on the formation of this product ion.

Fig. 5 shows four sections of product ion mass spectra between m/z = 26 and m/z = 29 upon bombardment of the propanethiol surface by Ar^+ (red dashed line) and N^+ (black line). In the case of Ar^+ all product ions fit perfectly to $C_2H_x^+$ ions (x = 2 to 5). The exact mass of these ions is indicated by thin, vertical, dashed, red lines. A small shoulder to the left of the peak at m/z = 29 is formed *via* N^+ collisions with propanethiol. This indicates a small amount of CNH_3^+ or N_2H^+. The poor signal to noise ratio does not allow a clear assignment of one of these ions. N_2^{2+} is isobaric to N^+ and is formed by double electron ionization of N_2 in the ion source.[39] From the isotopic contribution of $^{14}N^{15}N^{2+}$ at m/z = 14.5, we determined the relative amount of N_2^{2+} at m/z = 14 (see ESI,‡ Fig. S4). At an electron energy of 50 eV the molecular dication of nitrogen contributes about 5% to the yield of the projectile ions at m/z = 14. Upon surface collision, a small fraction of the molecular dication can capture one electron and add to the ion yield at m/z = 28. N_2^+ also agrees well with the position of this peak. The peak at m/z = 27 is strongly enhanced for the N^+ projectile and clearly wider and shifted to lower m/z values compared to the Ar^+ projectile ion. This agrees well with a substantial contribution of HCN^+ to $C_2H_3^+$ with a ratio of about 3 : 1.

All projectile ions react preferentially with the C3 carbon chains of the propanethiol surface and form in this mass range as product ions the hydrocarbons $C_2H_5^+$ at m/z = 29 and $C_2H_3^+$ at m/z = 27 in collisions with Ar^+. In collisions with N^+ and N_2^+ the increased intensity of m/z = 27 indicates, besides the presence of sputtered $C_2H_3^+$, efficient formation of HCN^+ in surface chemical reactions.

Fig. 6 shows the ratio of the ion yields at m/z = 27 and m/z = 29 from collisions of Ar^+, N^+, and N_2^+ in dependence on the projectile ion energy. It can be seen that in the case of Ar^+ collisions the ratio increases in the collision range from 5 eV to

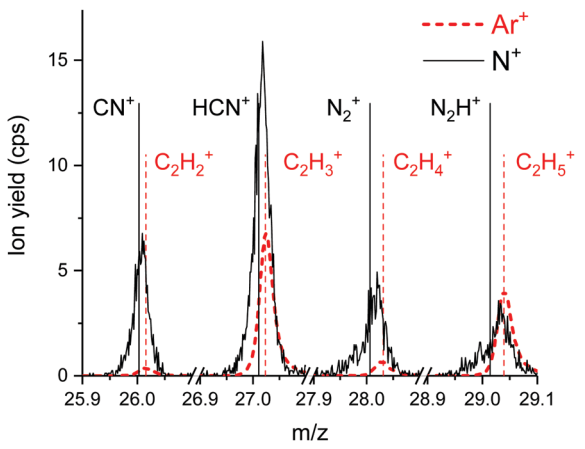

Fig. 5 High resolution mass spectra of product ions formed by N^+ (solid black line) and Ar^+ (red dashed line) projectiles on propanethiol at 69 eV impact energy. The higher relative yield at m/z = 27 for the N^+ projectile can be assigned to the formation of HCN^+.

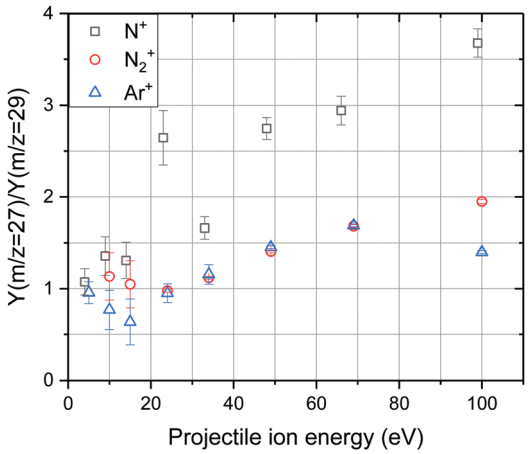

Fig. 6 Ratios of the ion yields at m/z = 27 and m/z = 29 as a function of the collision energy for the three projectile ions N^+ (black squares), N_2^+ (red circles) and Ar^+ (blue triangles). The data points were calculated by the arithmetic mean value of several measurements. The error bars were determined from the statistical error of ion counting and Gaussian error propagation. All measurements were carried out on a fresh 1-propanethiol SAM surface with irradiation times shorter than 15 minutes.

100 eV from less than 1 to about 1.5. N_2^+ exhibits the same energy dependence as Ar^+ up to a collision energy of 70 eV but reaches a value of almost 2 at 100 eV. In the case of N^+ collisions this ratio increases from about 1 to almost 4 in the same collision energy range. The data were then treated in the following way. The corrected yield of HCN^+ was calculated *via*

$$Y(HCN^+)_{N^+} = \frac{Y(27)_{N^+} \times Y(29)_{Ar^+}}{Y(29)_{N^+}} - Y(27)_{Ar^+}. \quad (1)$$

Similarly, the data for N_2^+ collisions were treated. The values of $Y(HCN^+)$ are plotted in Fig. 7.

The resulting set of points for N_2^+ collision shows values for low incident energies that scatter around zero and a strong increase for values above about 60 eV. The strong increase above 60 eV is the same as observed in collisions of N_2^+ with hydrocarbons from the residual gas adsorbed on metal surfaces.[20] This was interpreted as a surface reaction with an activation energy of 3–3.5 eV,[20] assuming the fraction of translational-to-internal energy transfer of 6/8% as determined earlier.[40,41] We stick to this interpretation here, too.

In collisions with N^+ the value of $Y(HCN^+)$ is quite high over the energy range from 100 eV down to 24 eV (Fig. 7), then it steeply decreases below about 20 eV and it is practically zero at 5 eV. This indicates that in collisions of N^+ with the propanethiol surface (C3 linear hydrocarbons), the heterogeneous reaction of HCN^+ formation has a very low threshold of a few tenths of an eV. Such a threshold would, obviously, prevent the reaction of HCN^+ formation between thermal N^+ ions and putative C3 hydrocarbons in the ionosphere of relevant astrophysical objects to occur. However, the propanethiol surface is only an artificial laboratory system and the heterogeneous reaction with aerosols of the tholin-type may still be possible.

In collisions with the background hydrocarbons[20] the values remained also quite high down to 20 eV, the lowest energy

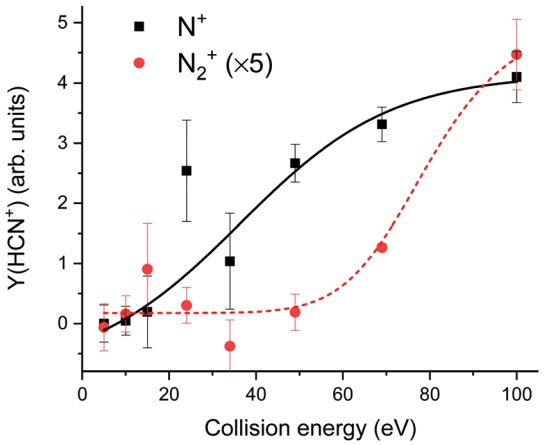

Fig. 7 HCN^+ yield at m/z = 27 ascribed to reactive surface collisions of N_2^+ (red circles) and N^+ (black squares) ions at different impact energies with a propanethiol SAM surface. The contribution of $C_2H_3^+$ was subtracted from the measured ion yield *via* eqn (1). The lines are two logistic fits of the form $y = A_2 + (A_1 - A_2)/(1 + (x/x_0)^p)$ to guide the eye.

measured. We do not know, if they remained high even at lower energies (as we assumed) or if they decreased to zero, similarly as in the experiments described here, because no data exist for the energy range below 20 eV. As the background hydrocarbons from cracked pump oil may contain, beside the linear C7 an C8 hydrocarbons also hydrocarbons with multiple bonds, *etc.*, $Y(HCN^+)$ may remain large even at very low incident energies.

Conclusions

(1) Collisions of N^+ and N_2^+ with C3 hydrocarbons represented by a self-assembled monolayer of propanethiol on a polycrystalline gold surface showed formation of HCN^+ at incident energies above a threshold energy for both projectile ions.

(2) In the case of N_2^+ bombardment the yield of HCN^+, increased above zero only at incident energies of about 60 eV. This suggests an activation energy of about 3–3.5 eV, assuming the earlier determined fraction of translational-to-internal energy transfer of 6–8%.[40,41]

(3) In the case of N^+ collisions the yield of HCN^+ was large over most of the incident energy range, but decreased to zero at incident energies below 15 eV. This may indicate a very small threshold energy for the surface reaction between N^+ and C3 hydrocarbons. Such a threshold may have existed even for collisions with adsorbed hydrocarbons,[20] as below 20 eV there are no data available.

Conflicts of interest

There are no conflicts to declare.

Acknowledgements

This work is supported by the Friedrich Schiedel Foundation for Energy Technology 259564, "Reaktive Ionen-Oberflächenstöße" and the Austrian Science Fund (FWF) W1259-N27 "DK-ALM". F. H. Financial support has also been provided by KKKÖ (Commission for the Coordination of Fusion Research) in Austria at the Austrian Academy of Sciences (ÖAW). The computational results have been achieved using the HPC infrastructure LEO of the University of Innsbruck.

References

1 L. E. Snyder and D. Buhl, *Astrophys. J.*, 1971, **163**, L47–L52.
2 Y. Gao and P. M. Solomon, *Astrophys. J., Suppl. Ser.*, 2004, **152**, 63–80.
3 Y. Gao and P. M. Solomon, *Astrophys. J.*, 2004, **606**, 271–290.
4 M. J. Mumma and S. B. Charnley, in *Annual Review of Astronomy and Astrophysics*, ed. S. M. Faber and E. VanDishoeck, Annual Reviews, Palo Alto, 2011, vol. 49, pp. 471–524.
5 R. Moreno, A. Marten, H. E. Matthews and Y. Biraud, *Planet. Space Sci.*, 2003, **51**, 591–611.
6 R. J. Cicerone and R. Zellner, *J. Geophys. Res.: Oceans*, 1983, **88**, 689–696.
7 C. N. Matthews and R. D. Minard, *Faraday Discuss.*, 2006, **133**, 393–401.
8 K. Lodders and B. Fegley, *Icarus*, 2002, **155**, 393–424.
9 V. Vuitton, R. V. Yelle and V. G. Anicich, *Astrophys. J.*, 2006, **647**, L175–L178.
10 J. H. Waite, H. Niemann, R. V. Yelle, W. T. Kasprzak, T. E. Cravens, J. G. Luhmann, R. L. McNutt, W. H. Ip, D. Gell, V. De La Haye, I. Muller-Wordag, B. Magee, N. Borggren, S. Ledvina, G. Fletcher, E. Walter, R. Miller, S. Scherer, R. Thorpe, J. Xu, B. Block and K. Arnett, *Science*, 2005, **308**, 982–986.
11 M. A. Cordiner, N. A. Teanby, C. A. Nixon, V. Vuitton, A. E. Thelen and S. B. Charnley, *Astron. J.*, 2019, **158**, 14.
12 G. Israel, C. Szopa, F. Raulin, M. Cabane, H. B. Niemann, S. K. Atreya, S. J. Bauer, J. F. Brun, E. Chassefiere, P. Coll, E. Conde, D. Coscia, A. Hauchecorne, P. Millian, M. J. Nguyen, T. Owen, W. Riedler, R. E. Samuelson, J. M. Siguier, M. Steller, R. Sternberg and C. Vidal-Madjar, *Nature*, 2005, **438**, 796–799.
13 K. J. Zahnle, *J. Geophys. Res.: Atmos.*, 1986, **91**, 2819–2834.
14 J. P. Ferris and W. J. Hagan, *Tetrahedron*, 1984, **40**, 1093–1120.
15 T. Das, S. Ghule and K. Vanka, *ACS Cent. Sci.*, 2019, **5**, 1532–1540.
16 *NIST Chemistry WebBook*, https://webbook.nist.gov.
17 V. H. Diebeler and S. K. Liston, *J. Chem. Phys.*, 1968, **48**, 4765–4768.
18 O. May, D. Kubala and M. Allan, *Phys. Rev. A: At., Mol., Opt. Phys.*, 2010, **82**, 4.
19 M. Inoue, *J. Chim. Phys. Phys.-Chim. Biol.*, 1966, **63**, 1061–1071.
20 M. Harnisch, A. Keim, P. Scheier and Z. Herman, *J. Phys. Chem. A*, 2013, **117**, 9653–9660.
21 A. Keim, M. Harnisch, P. Scheier and Z. Herman, *Int. J. Mass Spectrom.*, 2013, **354**, 78–86.

22 M. Harnisch, P. Scheier and Z. Herman, *Int. J. Mass Spectrom.*, 2015, **392**, 139–144.
23 Z. Herman, M. Harnisch, L. Ballauf and P. Scheier, *Chem. Listy*, 2018, **112**, 701–707.
24 C. Mair, T. Fiegele, F. Biasioli, Z. Herman and T. D. Märk, *J. Chem. Phys.*, 1999, **111**, 2770–2778.
25 C. D. Bain and G. M. Whitesides, *Science*, 1988, **240**, 62–63.
26 C. Vericat, M. E. Vela, G. Benitez, P. Carro and R. C. Salvarezza, *Chem. Soc. Rev.*, 2010, **39**, 1805–1834.
27 L. A. Bumm, J. J. Arnold, M. T. Cygan, T. D. Dunbar, T. P. Burgin, L. Jones, D. L. Allara, J. M. Tour and P. S. Weiss, *Science*, 1996, **271**, 1705–1707.
28 R. K. Smith, P. A. Lewis and P. S. Weiss, *Prog. Surf. Sci.*, 2004, **75**, 1–68.
29 P. Chinwangso, A. C. Jamison and T. R. Lee, *Acc. Chem. Res.*, 2011, **44**, 511–519.
30 O. Gutierrez-Sanz, D. Olea, M. Pita, A. P. Batista, A. Alonso, M. M. Pereira, M. Velez and A. L. De Lacey, *Langmuir*, 2014, **30**, 9007–9015.
31 J. G. Smith and P. K. Jain, *Phys. Chem. Chem. Phys.*, 2016, **18**, 23990–23997.
32 H. Hinterwirth, S. Kappel, T. Waitz, T. Prohaska, W. Lindner and M. Lammerhofer, *ACS Nano*, 2013, **7**, 1129–1136.
33 P. Ballauf, F. Duensing, F. Hechenberger and P. Scheier, *Rev. Sci. Instrum.*, 2020, **91**, 19.
34 C. D. Bain, E. B. Troughton, Y. T. Tao, J. Evall, G. M. Whitesides and R. G. Nuzzo, *J. Am. Chem. Soc.*, 1989, **111**, 321–335.
35 J. P. Folkers, P. E. Laibinis and G. M. Whitesides, *Langmuir*, 1992, **8**, 1330–1341.
36 Q. M. Guo and F. S. Li, *Phys. Chem. Chem. Phys.*, 2014, **16**, 19074–19090.
37 C. Vericat, M. E. Vela and R. C. Salvarezza, *Phys. Chem. Chem. Phys.*, 2005, **7**, 3258–3268.
38 W. Azzam, A. Al-Rashdi, A. Subaihi, M. Rohwerder, M. Zharnikov and A. Bashir, *Phys. Chem. Chem. Phys.*, 2020, **22**, 13580–13591.
39 L. Sigaud and E. C. Montenegro, *Phys. Rev. A: At., Mol., Opt. Phys.*, 2018, **98**, 6.
40 J. Zabka, Z. Dolejsek and Z. Herman, *J. Phys. Chem. A*, 2002, **106**, 10861–10869.
41 S. B. M. Bosio and W. L. Hase, *Int. J. Mass Spectrom.*, 1998, **174**, 1–9.

